

Analysis of Seismogenic Damage in Bam, Iran, Using Envisat ASAR Data

Gustavo Arciniegas, Wietske Bijker, Norman Kerle, Valentyn Tolpekin
Department of Earth Observation Science
ITC - International Institute for Geo-Information Science and Earth Observation,
P.O. Box 6, 7500 AA, Enschede, the Netherlands
arciniegas06157@itc.nl, bijker@itc.nl, kerle@itc.nl, tolpekin@itc.nl

Abstract: Significant surface changes occur frequently as a result of natural hazard events, of which earthquakes are considered the deadliest and most destructive, affecting mainly man-made structures. The detection, mapping and assessment of earthquake-related urban damage are critical, particularly in remote or inaccessible areas. Spaceborne satellite data are obtained without the necessity of accessing a location, covering large areas. Especially spaceborne SAR's weather-and-sunlight independence makes it a potential tool for post-disaster structural damage assessment of urban areas.

In this research we use a series of Envisat ASAR images to assess the capacity of InSAR data for detecting urban damages caused by the occurrence a 6.6 magnitude earthquake in Bam, Iran, on December 26, 2003. We analyze InSAR properties, such as complex coherence and signal amplitude and their sensitivity to changes in ground surface and urban damage, both induced by an earthquake event. These changes, among other causes, lead to quantifiable decorrelation of InSAR data.

A number of methods for post-earthquake urban damage assessment using spaceborne SAR images have been proposed by several authors. Of these methods, pixel by pixel comparison and change detection of InSAR properties are reviewed and analyzed in this study to compare and evaluate both their actual potentials and limitations through validation. This is done through correlating available damage maps created after the earthquake by competent entities. From this analysis, we calculate and map InSAR properties and quantitatively isolate earthquake-related urban damage from other sources of decorrelation.

Keywords: InSAR, coherence, amplitude correlation, earthquake, urban damage assessment, Bam

1. Introduction

Earthquakes are considered the deadliest and most destructive of hazard events, which frequently result in numerous casualties and substantial losses in terms of infrastructure and socio-economic damage. Significant surface and structural changes are also typical consequences of seismogenic activities. Assessing earthquake-related damage both rapidly and accurately is a challenging task that authorities must face before making crucial emergency-response decisions following the event.

Spaceborne satellite data can be acquired at regular intervals without the necessity of accessing a study area and covering much larger areas than airborne platforms. Optical data, particularly high-resolution satellite imagery, have largely been used for post-disaster damage assessment e.g. [1], yet with restrictions to atmospheric conditions, cloud cover and sunlight. Overcoming such limitations, spaceborne Synthetic Aperture Radar (SAR) is a potential tool for post-disaster structural damage assessment of remote or inaccessible cloud-covered urban areas, at any acquisition time.

SAR data have been predominantly used in change monitoring because of their sensitivity to alterations of Earth's surface, such as changes in geometric structure, surface roughness, and moisture content. Another major distinction of spaceborne SAR from optical sensors, besides weather-and-sunlight independence, is the possibility to extract both height and change information of a target area through SAR interferometry (InSAR). InSAR makes use of both amplitude and phase information contained in the backscattered echoes of the returning signal [2]. By combining two SAR images of the same scene, but acquired from slightly different positions (different viewing angles), it is possible to measure the phase differences across the common overlapping area and depict them in an interferogram, which ultimately leads to obtaining height information. In general, applications of spaceborne InSAR technique can be divided into two major groups: topographic mapping of surfaces (generation of Digital Elevation Models) [3] and change mapping studies such as monitoring of earthquakes, landslides, volcanic activity, land subsidence, glacier dynamics and land type classification, particularly, urban environments monitoring and classification.

In this research, we use a series of pre- and post-earthquake Envisat ASAR images of Bam, Iran, to assess the capacity of InSAR data for detecting urban damages. On December 26, a 6.6 magnitude earthquake occurred in Bam, Kerman Province, southeastern Iran, killing approximately 27,000 people and heavily damaging the majority (85%) of its buildings, according to official reports. We assume that InSAR properties, such as complex coherence and signal amplitude have a quantifiable sensitivity to changes in ground surface and urban damage, both induced by an earthquake event. These changes, among other causes, lead to decorrelation of InSAR data. Decorrelation can be defined as the decrease of similarity between two different radar observations over the same area. In repeat-pass configuration, SAR data correlation can be degraded by factors such as thermal noise, lack of parallelism between the radar flight tracks, spatial baseline noise, and surface changes [2]. Large temporal separations between image

acquisition dates also imply correlation losses due to the so-called temporal effect. The present study focuses on the effects of an earthquake over urban areas, particularly man-made structures and their interaction with SAR pulses. We use the Doris InSAR processor to calculate and map InSAR properties. In this analysis, earthquake-related urban damage is isolated from other sources of SAR decorrelation.

2. Previous use of SAR data on urban studies and post-earthquake damage detection

In urban areas, man-made structures are likely to produce stronger and more stable backscattering compared to their surrounding landscape. Radar backscattering of urban areas is affected by the orientation, shape, size, and dielectric properties of buildings, roads, bridges, man-made structures in general, and construction materials of building roofs, walls and the surrounding ground. Comprehensive research has been conducted on decorrelation of ERS-SAR (C-band) data acquired over urban areas in time. Usai and Klees [4] used SAR pairs spanning intervals from one day up to 3-1/2 years to show that coherence values of areas containing man-made features tend to remain significantly stable. Weydahl [5] analyzed fluctuations of both coherence and amplitude values on urban and vegetated areas with SAR imagery for temporal separations of one day (tandem pair) and 35 days, and compare the decorrelation of urban features to that of vegetated areas, concluding that some man-made objects preserve their coherence despite atmospheric or seasonal changes. Indeed, this stability has been exploited for DEM refinement purposes by detecting and using the stable backscatter of natural or artificial (corner) reflectors, known as permanent scatterers [6] and found generally in both rocky terrain and urban areas, regardless of varying viewing geometries. Relevant parameters for this approach [7] are discussed for feasibility and accuracy of deformation monitoring studies.

Concerning earthquakes, numerous studies have been carried out using SAR images. Early studies by Massonet et al. [8] and Zebker et al. [9] effectively demonstrated the feasibility of InSAR technique in mapping the co-seismic ground displacement caused by the 1992 Landers earthquake in California, United States. Suga et al. [10] and Yonezawa and Takeuchi [11] used SAR decorrelation and coherence information from a pair of SAR images for detecting earthquake-related urban damage by building collapse, and suggested normalized differences of complex phase coherence and SAR intensity to detect these changes. Matsuoka and Yamazaki [12] analyzed spectral characteristics and backscattering properties of areas damaged by earthquakes to distinguish several damage levels and also proposed change detection on collapsed buildings from SAR images. Bignami et al. [13] developed a method that combines SAR and optical satellite based data by computing complex coherence, intensity change and intensity-correlation coefficient from SAR pairs of the same scene and performing pixel-by-pixel change detection using optical data as training.

Recent studies [14] [15] used the Bam Envisat ASAR dataset and InSAR technology to map fault ruptures and surface displacement caused by the 2003 Bam earthquake. Regarding urban damage assessment, the former authors compute interferometric correlation (coherence) images, and map their differences to interpret visually their spatial characteristics in comparison to actual ground truth damage maps of Bam. No validation or detailed comparison was shown for building damage due to the lack of detail of their ground-truth data.

In most cases, a pre-seismic co-registered pair of SAR images is correlated, i.e., maintains similar ‘speckle’ patterns [2], or at least has higher correlation than a co-seismic pair. As a result of earthquake events, damage is induced on urban areas. In particular in severely damaged areas, building-geometry alterations and changes in surface are indeed present, leading to high decorrelation of the strong backscatter that urban areas tend to generate, compared to their surroundings. These variations may be related to changes in InSAR properties. Previous studies [16] suggest that amplitude values are in fact affected by an earthquake and that intensities of backscattering echoes (squared amplitude values) coming from intact buildings are considerably larger (or different) than those of collapsed buildings, open spaces or debris, given their randomly spatial arrangement and orientation. This study aims at analyzing such assumptions by using the Bam SAR dataset.

3. Resources and methodology

1) The 2003 Bam earthquake

With an urban area of 19.5 km² and a population of approximately 100,000 inhabitants, the historical city of Bam is located between the Jebalbarez and Kabudi Mountains on a flat and dry area. Geographically, Bam is situated between latitudes 29° to 29°15' N and longitudes 58°10' to 58°35' E, at an altitude of 1,050 meters above sea level (Fig. 1). Originally, Bam was a fortress called Arg-e-Bam, which would eventually become its most remarkable and historic feature: a mud-brick citadel complex, the biggest in the world (about 6 km² in area), founded during the Sassanian (Persian) period around 2,000 years ago and residential until 150 years ago. Arg-e-Bam was considered the second most splendid construction in the world prior to the earthquake, and it is registered as cultural remains on the UNESCO world’s heritage list.

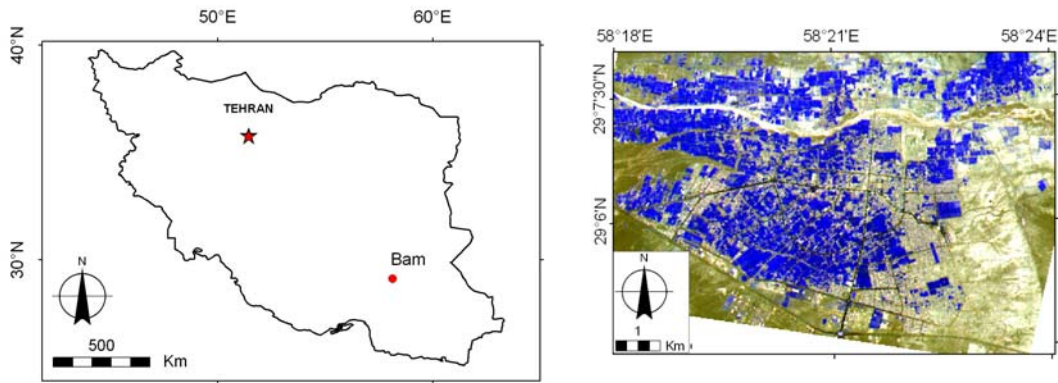


Fig. 1: Geographic location of Bam, Iran (left) and an ASTER false-color composite (FCC) image subset of Bam (right)

On December 26, a 6.6 magnitude earthquake occurred unannounced in Bam at 05:26 local time, 07:56 hours GMT, having its epicenter (29.01°N, 58.34°E) located approximately 10 km southwest of Bam [17]. According to the Iran's official statistics centre, 26,271 people were killed, 30,000 injured and 75,200 left homeless. In terms of human cost, the Bam earthquake ranks as the worst recorded disaster in Iranian history. Most of this destruction was concentrated on Bam: 85% of the buildings were damaged or destroyed by the event. More specifically, as reported by a United Nations' damage assessment team, 90% of buildings in Bam sustained 60-100% damage, that is, some 25,000 of the 29,500 structures within the city center and surrounding villages. The remaining building stock recorded 40-60% damage [18]. Its famous and ancient citadel was practically destroyed. For detailed information on the earthquake, refer to Nadim et al. [19]. The National Cartographic Center of Iran (NCC) prepared a damage distribution map, available at Earthquake Engineering Research Institute's website or at the National Geoscience Database of Iran's website [20]. It presents urban damage as three classes: 80-100% of destruction in purple, 50-80% of destruction in red and 20-50% of destruction in yellow (Fig. 2, left). This map, used as 'ground truth' information for validation purposes of this study, does not contain detail of damage at the scale of individual buildings. It shows instead three damage classes outlined per city block in Bam, classifying vegetated areas also as damaged zones (Fig. 2, right). Historical precipitation data of Bam [21], a potential source of decorrelation, show that negligible precipitation occurred in Bam at the earthquake moment and between the SAR acquisitions dates.

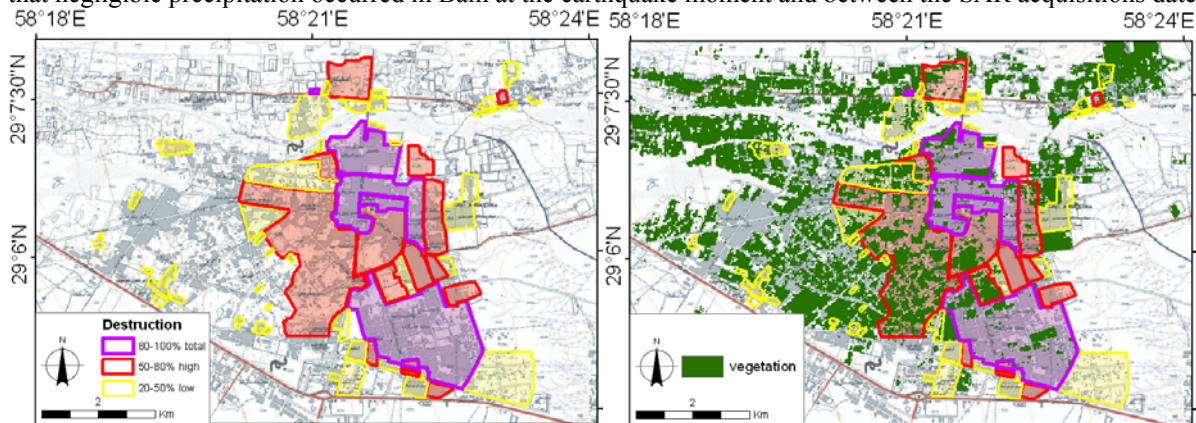


Fig. 2: Ground truth data (left) and existing vegetation in Bam overlaid with ground truth damage outlines (right)

2) Remote sensing images: ASAR and ASTER

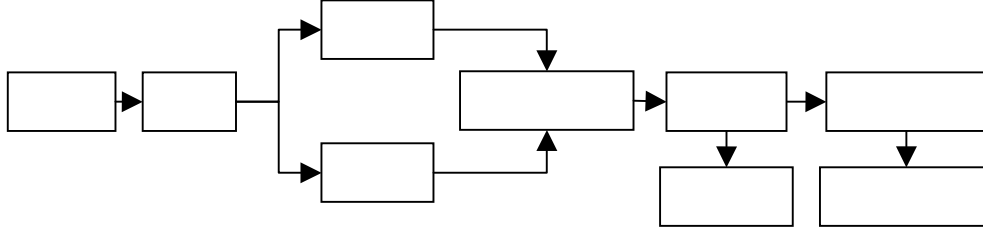
The Envisat satellite (35-day repeat period) observed the city of Bam, acquiring SLC-format images in descending pass centering on the city with the ASAR sensor (C-band, VV polarization) at different moments before and after the earthquake. Each image has an azimuth (along track) resolution of 4 to 5 m and range (across track) resolution of 9 to 18 m, and covers 100 km along-track and 56-100 km across-track. Of the four images, three have been used in this study as shown in Table 1. The ASTER (Advanced Spaceborne Thermal Emission and Reflection Radiometer) instrument, mounted on the Terra satellite, imaged the city of Bam on May 5, 2003, 234 days before the Bam earthquake's occurrence. Three bands (1, 2 visible and 3N near-infrared) are available for this study. Fig. 1 shows a subset of the ASTER image (false-color composite, 15 m of spatial resolution) covering the city of Bam. Bam is significantly covered by vegetation, mostly date plantations and palm grove, appearing as blue areas on the image.

Table 1: ASAR dataset used in this study

Name	Orbit	Acquisition date	Days before/after earthquake
B1	6687	11/Jun/2003	198 days before
B2	9192	03/Dec/2003	23 days before
A1	9693	07/Jan/2004	12 days after

3) Interferometric processing

The InSAR processing (Fig. 3) of this study was performed using the freely-available Delft Object-oriented Radar Interferometric Software (DORIS) [22], developed at the Department of Earth Observation and Space Systems (DEOS), Delft University of Technology, the Netherlands.

**Fig. 3: major steps of the InSAR processing in this study**

The Envisat SLC ASAR data format is read and subsets delimiting Bam city are extracted at full resolution from the three images. Each image has a pre-processing size of 5,167 by 26,000 pixels, and each subset has a size of 1500 x 7500 pixels (range and azimuth respectively). Multi-looking is applied to yield approximately square pixels of about 20 meters, to decrease noise and to reduce speckle, at the cost of resolution. In this process, data are averaged by a specified window at a certain factor, i.e. window size. In this study, a multi-looking factor of 1 in range and 5 in azimuth was used, yielding an image size of 1500x1500 multi-looked 20x20-meter-square pixels, a minimum square-pixel resolution that can be obtained from ASAR SLC images.

Concerning spaceborne sensors, the baseline (B) is the geometric separation between two antenna positions in two ideally parallel satellite orbits [23]. Geometrically, it is an important InSAR parameter because if too short, the sensitivity to signal phase differences will be undetectable; while if too long, additional noise to spatial decorrelation corrupts the signal [2]. The spatial baseline is separated into two components with respect to the range direction: perpendicular baseline B_{\perp} (effective distance) and parallel baseline B_{\parallel} . Its length determines the suitability of a SAR dataset for InSAR processing. For Envisat ASAR, theoretically, the critical value of B_{\perp} is 1,100 m; however for practical applications (InSAR limit) it should be less than 600 m for flat terrain [24]. The temporal baseline B_{temp} , or time span between two observations, plays a major role if changes (e.g. due to hazard events) are to be analyzed, as SAR data lose correlation due to different reasons. High correlation (between two SAR images) may be achieved only when hardly any environmental [3], seasonal or man-made changes occur. Table 2 shows computed baselines of the Bam's dataset.

The InSAR processing requires two or more SAR images to be accurately registered to a common reference, i.e. master, during co-registration stage. Azimuth spectrum filtering is applied to master and slave in order to filter out parts that do not overlap. This filtering improves coherence, particularly for interferograms with a long temporal baseline where co-registration is difficult due to low coherence [4], like that of this study's pre-seismic Bam pair. Image B2 (03/Dec/2003) is selected as master image, meaning that other images B1 and A1 were registered to B2 and resampled into its reference grid. Having both images share the same grid, phase differences between corresponding pixels are mapped in an interferogram. Pre-seismic and co-seismic pairs of SAR images are defined as follows: a pre-seismic pair consisting of two SAR images both acquired before the earthquake and a co-seismic pair comprising two SAR images that span the earthquake's occurrence (See Table 2).

Table 2: Pre-seismic and co-seismic pairs and their computed baselines from the dataset

Pair	Images	B(m)	B_{\perp} (m)	B_{\parallel} (m)	B_{temp} (days)
Pre-seismic	B2-B1	496.5	473.6	148.6	175
Co-seismic	B2-A1	586.2	516.3	277.6	35

The complex interferometric coherence is a measure of correlation between two SAR images, which can be calculated from an interferogram. The complex coherence γ between two zero-mean circular Gaussian variables y_1 and y_2 is defined in Hanssen [25] as

$$\gamma = \frac{E\{y_1, y_2^*\}}{\sqrt{E\{|y_1^2|\} \cdot E\{|y_2^2|\}}}, \quad 0 \leq \gamma \leq 1. \quad (1)$$

E is the expectation (ensemble averaging) operator over which coherence is estimated and then assigned to every co-registered pixel. Coherence $g_{(M,S)}$, between both complex master M and complex (resampled) slave S , is a function of phase and amplitude, and is defined by $|g_{(M,S)}|$ [22] and its estimator $\hat{\gamma}$ as:

$$\hat{\gamma} = |g_{(M,S)}| = \frac{E\{M \cdot S^*\}}{\sqrt{E\{M \cdot M^*\} \cdot E\{S \cdot S^*\}}} = \frac{\frac{1}{N} \sum M \cdot S^*}{\sqrt{\frac{1}{N} \sum M \cdot M^* \cdot \frac{1}{N} \sum S \cdot S^*}}, \quad 0 \leq \hat{\gamma} \leq 1 \quad (2)$$

Here, $*$ is the complex conjugated (master or slave). In this estimation, summations are calculated over N pixels in a 5×5 window and multi-looking (1:5) is performed thereafter to reduce noise. Ranging from 0 to 1, coherence values indicate, respectively, how incoherent or coherent two co-registered images are. These values are mapped for corresponding master-slave pixels with DORIS, showing bright pixels as coherent (similar) and dark pixels as incoherent (dissimilar). A number of parameters strongly influence the coherence losses, for example atmospheric conditions, vegetation, spatial baseline and temporal separation. Changes, particularly caused by earthquake events apparently lead to coherence losses. Fig. 4 shows subsets of amplitude images for the pre-earthquake master and the post-earthquake image and coherence images for pre-seismic and co-seismic pairs.

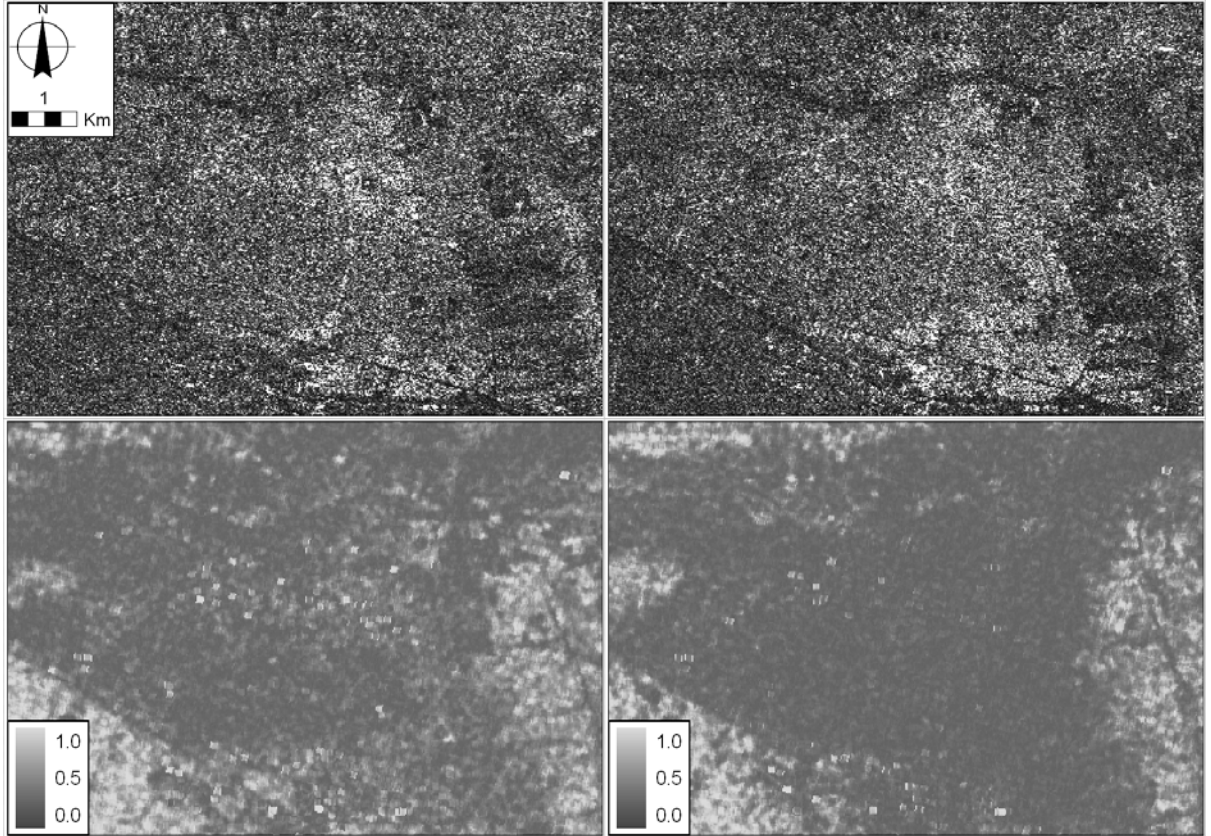


Fig. 4: (Top) amplitude images of Bam acquired before the earthquake (left) on 03/Dec/2003 and after the earthquake (right) on 07/Jan/2004. (Bottom) coherence images for pre-seismic (left) and co-seismic (right) SAR pairs

4. Results: correlation between building damage and InSAR properties

The available ground-truth damage distribution map is co-registered to the unique master image B2 (03/Dec/2003), re-scaled and resampled at its same resolution of 20 meters to produce a raster image. As a result, a 37,580-cell raster image is produced, indicating three damage levels of the Bam earthquake, assigned to each pixel. 37,580 points are then generated for each raster cell and related to corresponding values of coherence (pre- and co-seismic) and amplitude (pre- and post-earthquake) through layer intersection. This resolution is not enough to

visually or statistically evaluate urban damage at the precision of individual buildings, but in this study it has been assumed that damage distribution per city block can be assessed at this resolution through pixel by pixel comparison.

Box-plots are created as an attempt to describe the distribution of the entire urban damage point set, and to find patterns that may be associated to decorrelation resulting from earthquake damage. Each graph presents one of computed InSAR properties in the y axis and three classes of urban damage in the x axis, according to available ground truth data. The three classes correspond to total, high and low damage, respectively.

1) Analysis of phase coherence

Pre-seismic and co-seismic coherence values, computed in a 5x5 estimation window, are mapped and geocoded using parameters in UTM zone 40, WGS-84 datum, for corresponding 20-m resolution pixels, in the urban area of Bam (Fig. 4, bottom). Pre-seismic coherence values are low, mostly due to both the long temporal separation (175 days) and the existence of vegetation in Bam. Nevertheless, some bright clusters with relatively higher coherence appear in the image, corresponding to built-up areas which suffered less decorrelation during pre-seismic acquisitions. As for the co-seismic pair, coherence values drop with respect to pre-seismic ones, indicating losses, mostly in those areas which appeared bright in the pre-seismic pair. Clearly, values decrease as a result of decorrelation induced by changes which occurred during 35-day period between acquisitions and changes caused by the earthquake.

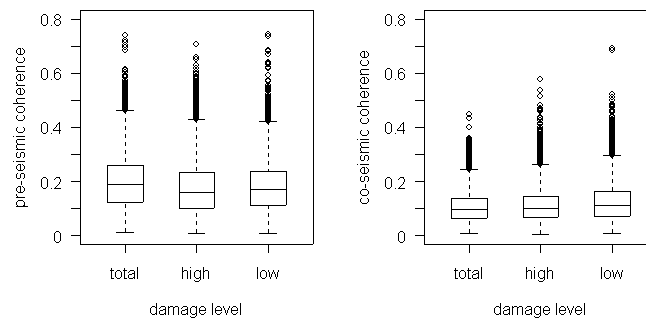


Fig. 5: Box-plots of coherence vs. ground truth damage level for pre-seismic (left) and co-seismic pairs (right). 'Total' corresponds to 80-100% of destruction, 'high' to 50-80% and 'low' to 20-50%

Fig. 5 shows box-plots for both computed pre-seismic and co-seismic coherence values vs. urban damage level. Comparing the two plots, coherence values are lower in the co-seismic pair, which includes the earthquake's occurrence, for both main data spread and outliers. Evidently, besides the long spatial co-seismic baseline, the decrease in coherence values can be associated with the earthquake's occurrence despite the already low pre-seismic coherence. Points in the 'total destruction level' class have slightly lower co-seismic coherence values, if compared to the other two classes. In fact, there is a small trend as coherence values tend to decrease with increasing damage level. In conclusion, as a result of the earthquake, comparatively high-coherence pixels (mostly intact built-up areas) become lower-coherence pixels (areas containing collapsed buildings). This could serve as a rough estimate of severely damaged areas.

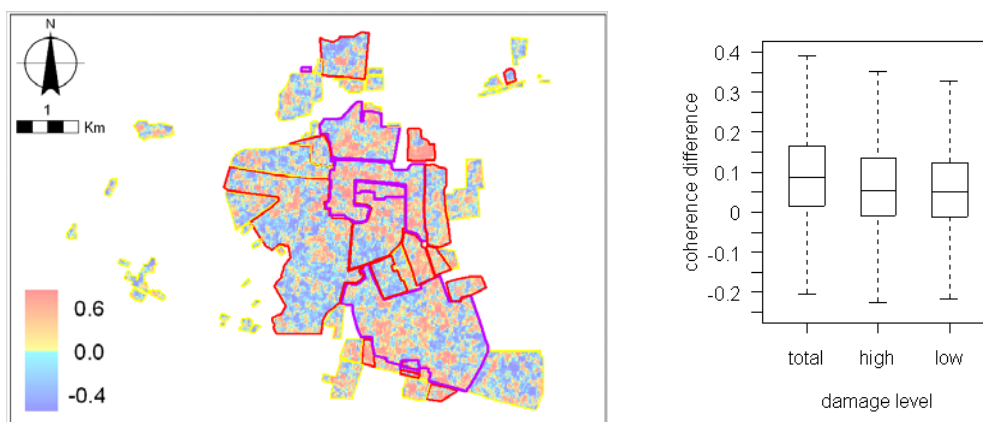


Fig. 6: Coherence difference map overlaid with ground-truth damage outlines (left) and box-plot of coherence differences vs. ground truth damage level (right)

Both pre-seismic and co-seismic coherence maps are subtracted to create a difference map (Fig. 6, left). Visually, pixels with high coherence differences can be identified inside Bam's urban area. Some of these pixels form clusters, which to some extent resemble actual collapsed-buildings areas, when overlaid with the purple outlines of

ground-truth actual damage (Fig. 6, left). These differences are plotted vs. urban damage level (Fig. 6, right). This plot shows that points associated with total destruction have the largest values of coherence differences. The total building damage class stands out from the other two classes in terms of coherence differences. In other words, areas containing collapsed buildings may show the largest drops in coherence because coherence changes are highly susceptible to changes in height, which is the case if intact buildings become rubble due to an earthquake. Points with high destruction level have slightly larger coherence losses than those with low destruction level, but this difference is not as remarkable as that related to total destruction.

2) Analysis of signal amplitude

Signal amplitude values are mapped and compared for two images acquired before (03/Dec/2003) and after (07/Jan/2004) the earthquake. By visually comparing both amplitude images (Fig. 4, top), it is obvious that the strength of the signal changes all over Bam after the earthquake. Fig. 7 presents box-plots of pre- and post-earthquake amplitude values vs. damage level. In the image acquired after the earthquake, amplitude values tend to be higher (main spread and maximum values) than those of the pre-earthquake image, but neither increases nor decreases in amplitude can be attributed to the earthquake.

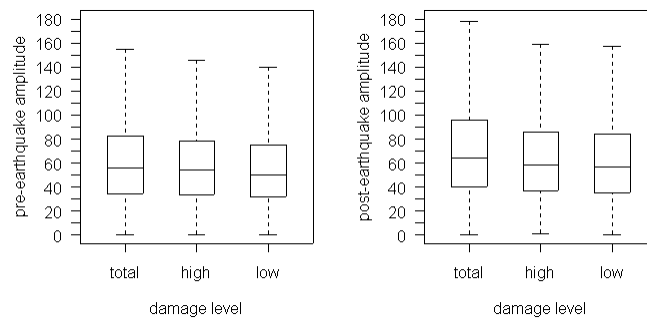


Fig. 7: Box-plots of amplitude vs. ground-truth damage level for pre- (left) and post-earthquake (right) SAR images

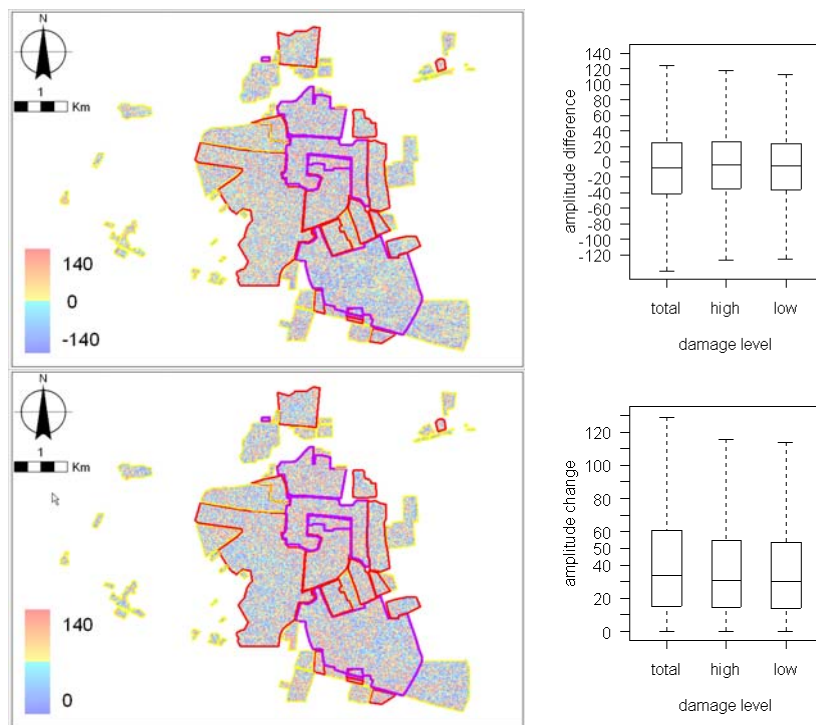


Fig. 8: (Top) amplitude difference map (left) and box-plot vs. ground truth damage level (right). (Bottom) amplitude change map (left) and box-plot vs. ground truth damage level (right). Both maps are overlaid with ground truth damage outlines

Amplitude differences between pre- and post-disaster images are calculated and mapped. In addition, absolute values are taken, so that no negative differences appear (See Fig. 8). These two maps are compared because, unlike complex coherence, earthquake effects can be reflected in either drop or rise of amplitude value for corresponding pixels. Pixels containing collapsed buildings or cleared areas may be corner reflectors or flat surfaces, appearing in

the bright or dark respectively. It is not possible to state that the amplitudes of the returning signal coming from collapsed buildings or debris are always higher or lower those of intact buildings. Differences in amplitude are therefore plotted vs. damage level (Fig. 8). Points related to total-damage level correspond to larger differences in amplitude.

3) An attempt to extract damaged areas and validation of the results

An effort to extract damaged areas from the calculations above was made by using coherence differences and amplitude changes to assign a damage class to each pixel. Thresholds are set by using both box-plots created to separate ‘total’ and ‘high’ damage classes from low damage class. Fig. 9 shows the classification results overlaid with ‘ground truth’ damage outlines. Both ‘total’ and ‘high’ destruction levels have been renamed as ‘total and high’ whereas the ‘low’ class remains the same. To quantify which InSAR property best resembles both total and high damage levels, an error (confusion) matrix was created for each of the classifications (Tables 3 and 4).

Table 4 contains the highest overall accuracy (44.5%), corresponding to a classification made using coherence differences, although both overall accuracy values are not high. When trying to classify correctly both total and high damage levels, coherence differences seem to work better than amplitude changes, according to the slightly smaller omission errors (4.4 % difference). On the other hand, if undamaged areas are to be extracted, the two properties work almost equally well, but this is less relevant for this study. Hence, producer accuracies are relatively high because many undamaged pixels have been correctly classified compared to damaged pixels. This may be a consequence of the existence of vegetation in Bam and the fact that the ground truth map contains vegetation areas classified as damage, due to its lack of detail.

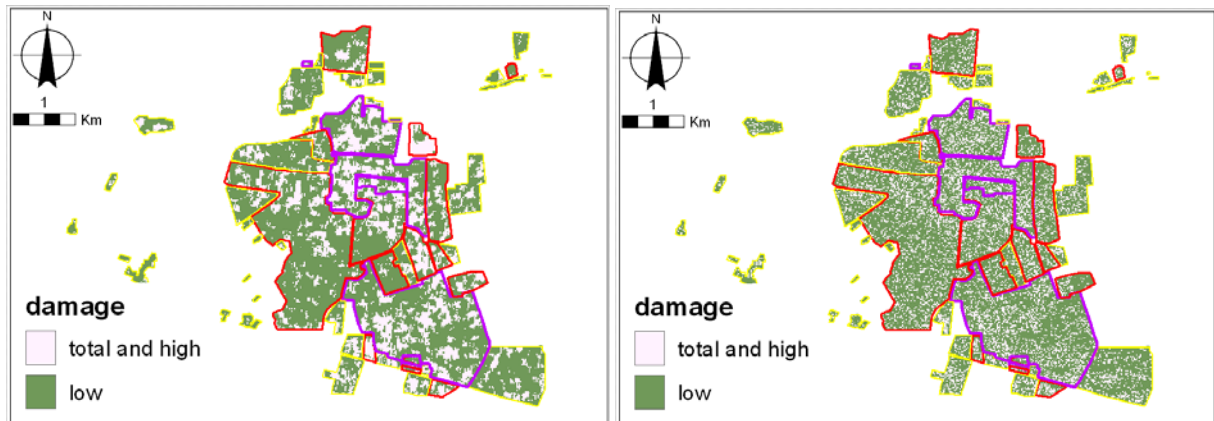


Fig. 9: Classification results for damage extraction by using coherence differences (left) and amplitude change (right). Both maps are overlaid with ground truth damage outlines

Table 3: Error matrix for amplitude change, reference classes in the top row and classification results in the leftmost column, overall accuracy = 41.2%

	Total and high	Low destruction	Total	Error of Commission (%)	User Accuracy (%)
Total and High	7402.0	2679.0	10081.0	26.6	73.4
Low	19426.0	8073.0	27499.0	70.6	29.4
Total	26828.0	10752.0	37580.0		
Error of Omission (%)	72.4	24.9			
Producer Accuracy (%)	27.6	75.1			

Table 4: Error matrix for coherence change, reference classes in the top row and classification results in the leftmost column, overall accuracy = 44.5%

	Total and high	Low destruction	Total	Error of Commission (%)	User Accuracy (%)
Total and High	8590	2624	11214	23.4	76.6
Low	18238	8128	26366	69.2	30.8
Total	26828	10752	37580		
Error of Omission (%)	68	24.4			
Producer Accuracy (%)	32	75.6			

4) Effect of vegetation

Thus, we analyzed the effect of existing vegetation in Bam, using the ASTER image (Fig. 1, right). A vegetation mask has been created through band slicing (Fig. 2, right) and the same analysis has been implemented using now a masked damage map which may describe damage in Bam in better detail. Points are again related to InSAR properties computed in this study. Fig. 10 shows that both ‘total and high’ classes can be better discriminated from ‘low’ class. Pixels with vegetation are removed and coherence values slightly increase. By classifying coherence differences using box-plot thresholds, a slightly better overall accuracy value is obtained (Table 5) and both ‘total’ and ‘low’ destruction is extracted with higher accuracy.

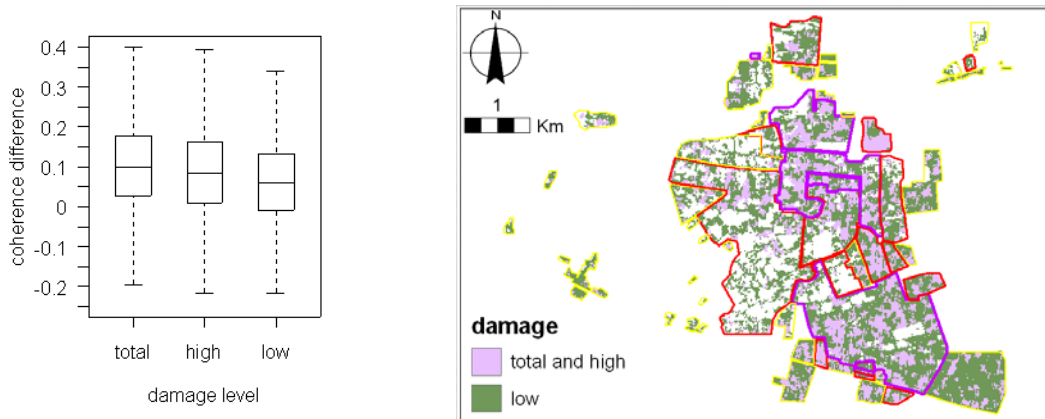


Fig. 10: (Left) Box-plot of coherence differences vs. ground truth damage level. (Right) Classification results for damage extraction using coherence differences, overlaid with ground truth damage outlines, vegetation discriminated

Table 5: Error matrix for coherence differences, vegetation discriminated. Reference classes in the top row and classification results in the leftmost column, overall accuracy = 48.7%

	Total and high	Low destruction	Total	Error of Commission (%)	User Accuracy (%)
Total and High	7162.0	2165.0	9327.0	23.2	76.8
Low	12123.0	6401.0	18524.0	65.4	34.6
Total	19285.0	8566.0	27851.0		
Error of Omission (%)	62.9	25.3			
Producer Accuracy (%)	37.1	74.7			

5. Conclusions and Discussion

Coherence and SAR amplitude information have been related to earthquake-induced urban damage. Changes have been analyzed, first visually and then quantitatively through classification and validation. Coherence works relatively better than amplitude in extracting damaged areas as it discriminates total destruction better. However, there is no conclusive evidence that suggests that a full assessment of earthquake-related urban damage can be made with SAR images as the only source of information.

SAR data have an important sensitivity for measuring surface changes at the range of microwaves. Based on earlier studies, it is assumed that collapsed buildings or heavily damaged areas have different backscattering properties than undamaged areas. But empty spaces, vegetated areas or rubble/debris can also have different backscattering properties, which may be similar to those of collapsed buildings. SAR datasets have been previously used to classify urban damage into several levels. In this study, such classification has not been achieved. As a general limitation, it is not feasible to classify damage accurately into several levels. Earthquake destruction leads to high decorrelation on SAR data, but several other factors might as well pose influences that may be wrongly attributed to the event, such as changes in vegetation, atmospheric and seasonal changes, and long temporal baseline.

Another possible reason for this discrepancy is that the ‘ground truth’ information used in this research was not the appropriate reference for this type of study. It seems that this damage map was made for different purposes as a result of a visual interpretation of urban damage at a more general scale (blocks of buildings), rather than a detailed report of individual-building damage. In other words, this map could possibly have been made with the purpose to communicate the impact of the earthquake in terms of major damage per neighborhood. This information is not enough, if it is intended to be used as a comparison to what a SAR sensor measures.

It appears to be a very difficult task to separate earthquake-induced changes from those related to other causes. Moreover, it seems to be even more difficult to separate damage classes with SAR data. Further studies should be conducted on how to differentiate earthquake-related decorrelation of SAR data quantitatively and qualitatively, from other sources of decorrelation of these types of data in urban areas. In addition, it is also recommended to study how

the use of SAR data can complement current methods that use optical images, stressing on features that stand out above those of optical images. The SAR backscattering behavior of urban areas with heterogeneous building stock or uniformity in building height should be studied as well. It is important to choose pairs of SAR data which are suitable in terms of baseline and time gap, although there is not a definite rule about the optimal values of spatial baselines for the urban domain. Spatial baseline values can be studied with the purpose to define optimal values for studies related to urban-domain applications, for different SAR sensors.

Acknowledgments

We thank Tsehaie Woldai for access to the ASAR data and valuable discussions.

References

- [1] Yamazaki, F., K.i. Kouchi, M. Matsuoka, M. Kohiyama, and N. Muraoka, 2004. Damage detection from high-resolution satellite images for the 2003 Bourmedes, Algeria earthquake. in 13th World Conference on Earthquake Engineering. Vancouver, B. C., Canada.
- [2] Zebker, H.A. and J. Villasenor, 1992. Decorrelation in Interferometric Radar Echoes. *IEEE Transactions on Geoscience and Remote Sensing*, 30(5): p. 950-959.
- [3] Zebker, H.A., C.L. Werner, P.A. Rosen, and S. Hensley, 1994. Accuracy of Topographic Maps Derived from ERS-1 Interferometric Radar. *IEEE Transactions on Geoscience and Remote Sensing*, 32(4): p. 823-836.
- [4] Usai, S. and R. Klees, 1999. SAR interferometry on a very long time scale: a study of the interferometric characteristics of man-made features. *Geoscience and Remote Sensing, IEEE Transactions on*, 37(4): p. 2118-2123.
- [5] Weydahl, D.J., 2001. Analysis of ERS SAR coherence images acquired over vegetated areas and urban features. *International Journal of Remote Sensing*, 22(14): p. 2811-2830.
- [6] Ferretti, A., C. Prati, and F. Rocca, 2001. Permanent scatterers in SAR interferometry. *Geoscience and Remote Sensing, IEEE Transactions on*, 39(1): p. 8-20.
- [7] Hanssen, R.F., 2005. Satellite radar interferometry for deformation monitoring: a priori assessment of feasibility and accuracy. *International Journal of Applied Earth Observation and Geoinformation*, 6(3-4): p. 253-260.
- [8] Massonnet, D., M. Rossi, C. Carmona, F. Adragna, G. Peltzer, K. Feigl, and T. Rabaute, 1993. The displacement field of the Landers earthquake mapped by radar interferometry. *Nature*, 364(6433): p. 138-142.
- [9] Zebker, H.A., P.A. Rosen, R.M. Goldstein, A. Gabriel, and C.L. Werner, 1994. On the derivation of coseismic displacement fields using differential radar interferometry: the Landers earthquake. *Journal of Geophysical Research*, 99(B10): p. 19,617-19,634.
- [10] Suga, Y., S. Takeuchi, Y. Oguro, A.J. Chen, M. Ogawa, T. Konishi, and C. Yonezawa, 2001. Application of ERS-2/SAR data for the 1999 Taiwan earthquake. *Advances in Space Research*, 28(1): p. 155-163.
- [11] Yonezawa, C. and S. Takeuchi, 2001. Decorrelation of SAR data by urban damages caused by the 1995 Hyogoken-nanbu earthquake. *International Journal of Remote Sensing*, 22(8): p. 1585-1600.
- [12] Matsuoka, M. and F. Yamazaki, 2004. Damage Detection of the 2003 Algeria using SAR Intensity Images. in 1st Asia Conference on Earthquake Engineering.
- [13] Bignami, C., M. Chini, N. Pierdicca, and S. Stramondo, 2004. Comparing and combining the capability of detecting earthquake damages in urban areas using SAR and optical data. in IEEE International Geoscience and Remote Sensing Symposium. Alaska, USA.
- [14] Fielding, E.J., M. Talebian, P.A. Rosen, H. Nazari, J.A. Jackson, M. Ghorashi, and R. Walker, 2005. Surface ruptures and building damage of the 2003 Bam, Iran, earthquake mapped by satellite synthetic aperture radar interferometric correlation. *Journal of Geophysical Research*, 110(B03302).
- [15] Stramondo, S., M. Moro, F. Doumaz, and F.R. Cinti, 2004. The 26 December 2003, Bam, Iran earthquake: surface displacement from Envisat ASAR interferometry. *International Journal of Remote Sensing*, 26(5): p. 1027 - 1034.
- [16] Matsuoka, M. and F. Yamazaki, 2000. Use of Interferometric Satellite SAR for Earthquake Damage Detection. in 6th International Conference on Seismic Zonation, EERI.
- [17] USGS. Poster of the Bam, Iran Earthquake of 26 December 2003 - Magnitude 6.6. Available at: <http://neic.usgs.gov/neis/poster/2003/20031226.html>
- [18] Adams, B.J., C.K. Huyck, M. Mio, S. Cho, S. Ghosh, H.C. Chung, R.T. Eguchi, B. Houshmand, M. Shinozuka, and B. Mansuori, *The Bam (Iran) Earthquake of December 26, 2003: Preliminary Reconnaissance Using Remotely Sensed Data and the VIEWS (Visualizing the Impacts with Satellite Images) System*, M.E.R.I. Report, Editor. 2004.
- [19] Nadim, F., C. Lindholm, S. Remseth, A. Andresen, and M. Moghtaderi-Zadeh, *Bam Earthquake of 26 December 2003 - ICG Reconnaissance Mission, in International Centre for Geohazards*. 2004, Geological Survey of Iran. p. 81.
- [20] NGDIR. National Geoscience Database of Iran. Available at: <http://www.ngdir.ir>
- [21] Weeronline.nl. Weeronline Bam Iran. Available at: <http://www.weeronline.nl/Iran/Bam.htm>
- [22] DEOS. Doris InSAR Processor. Available at: <http://enterprise.lr.tudelft.nl/doris/>
- [23] Gens, R., *Quality Assessment of SAR Interferometric Data*, in *Earth Observation Science*. 1998, University of Hannover: Enschede. p. 141.
- [24] Holzner, J., M. Eineder, and B. Schattler. First Analysis of Envisat/ASAR Image Mode Products for Interferometry. Available at: http://envisat.esa.int/calval/proceedings/asar/asar_19.pdf
- [25] Hanssen, R.F., *Stochastic model for radar interferometry*, in *Radar Interferometry. Data Interpretation and Error Analysis*, F.v.d. Meer, Editor. 2001, Kluwer Academic Publishers: Delft. p. 96-98.